

30-Hz-linewidth Watt output power 1.65 μm continuous-wave singly resonant optical parametric oscillator

Aliou Ly¹, Christophe Siour¹, and Fabien Bretenaker^{1*}

¹*Laboratoire Aimé Cotton, Université Paris-Sud,
ENS Cachan, CNRS, Université Paris-Saclay, Orsay, France*

We build a 1-Watt cw singly resonant optical parametric oscillator operating at an idler wavelength of 1.65 μm for application to quantum interfaces. The non resonant idler is frequency stabilized by side-fringe locking on a relatively high-finesse Fabry-Perot cavity, and the influence of intensity noise is carefully analyzed. A relative linewidth down to the sub-kHz level (about 30 Hz over 2 s) is achieved. A very good long term stability is obtained for both frequency and intensity.

PACS numbers:

I. INTRODUCTION

Building efficient quantum communication networks requires the implementation of quantum light-matter interfaces in the communication channels in order to overcome two major limitations. First, the attenuation of light in telecom C-band optical fibers significantly limits the reachable communication distances to few tens of kilometers at the single photon level. Second, the most efficient single photon detectors such as Si APDs lie into the visible range of the spectrum. Quantum memories for photons have then been proposed to increase the communication distances by allowing the synchronization of quantum relays. But it appears that the most efficient memories do not operate at telecom wavelengths [1].

To efficiently interface a memory to a telecom single photon source and take advantage of Si APDs, one can use quantum frequency conversion via nonlinear processes in a $\chi^{(2)}$ medium [2], which has been shown to be relatively efficient and to preserve the quantum state of the photon [3]. Since then, numerous experimental realizations involving single photon up-conversion and using the SFG scheme into a $\chi^{(2)}$ medium have been performed. For instance, a recent example is the demonstration of storage of up-converted telecom photons into a quantum memory for visible photons [4]. Cheng *et al.* have up-converted near-IR photons to the visible with practically no background photons [5]. Concerning non-classical Gaussian states, Vollmer *et al.* succeeded in up-converting squeezed vacuum states from 1550 to 532 nm [6].

In most of the experiments described above, single photon up-conversion is performed in periodically-poled lithium niobate (PPLN). Then one problem that arises is the noise that may exist at the up-converted wavelength even in the absence of single photons to be converted. A large part of this noise is due to anti-Stokes stimulated Raman scattering (SRS) in lithium niobate [7]. To overcome this limitation, several strategies were

explored. Some authors have tried to perform an efficient spectral filtering of the up-converted signal [8], while others have tried a cascaded single photon up-conversion [9]. But the most promising approach would be to pump at a wavelength much longer than that of the signal to be up-converted. Moreover, the availability of a broadly tunable pump would certainly make it easier to minimize the SRS noise for a given signal or up-converted wavelength. Moreover, although the frequency noise of the pump will not significantly affect the efficiency of the quantum interface [4], it might reduce the quantum memory efficiency depending on the used protocol. Up to now, the pump laser sources that have been used to up-convert near-infrared single photons are CW laser diodes [5], external-cavity diode lasers followed by a tapered amplifier [4], thulium fiber lasers amplified by a thulium doped fiber amplifier [10], or a monolithic optical parametric oscillator (OPO) combined with a fiber amplifier [7].

However, recently, it has been shown that the non resonant wave in a singly-resonant OPO (SRO) could be stabilized by transferring the pump noise to the resonant wave [11–13]. This permits to take advantage of the efficient power transfer from the pump to the non resonant wave while stabilizing the frequency noise below the pump frequency noise. Consequently, the aim of the present paper is to take advantage of this source architecture to build a stabilized SRO operating around 1.65 μm . We choose this wavelength as a test wavelength for up-converting photons at telecom wavelengths (typically around 1535 nm) to the wavelength of rubidium quantum memories (795 nm). In the second section, we describe the SRO we have built. The third section then reports the power, tunability, and mode quality of this SRO. Finally, section 4 is devoted to a study of the power and frequency stability of the OPO, with a comparison of free running and frequency locked operations.

II. DESCRIPTION OF THE OPO

The experimental setup is depicted in Fig. 1. The SRO is pumped at 532 nm by a cw 10 W single-frequency Co-

*Electronic address: Fabien.Bretenaker@u-psud.fr

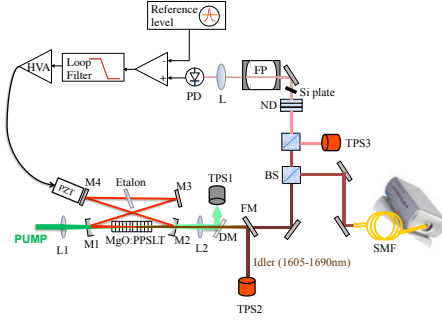


FIG. 1: Schematic of the experimental setup. HVA: high-voltage amplifier. PZT: piezoelectric transducer. PD: Photodiode. L: focusing lens. FP: Fabry-Perot cavity. DM: Dichroic Mirror. BS: Beamsplitter Cube. ND: Neutral Density. TPS: Thermal Power Sensor. FM: Flippable Mirror. SMF: Single-Mode Fiber.

herent Verdi laser and is based on a 30-mm long MgO-doped periodically poled stoichiometric lithium tantalate (PPSLT) crystal ($d_{\text{eff}} \approx 11 \text{ pm/V}$) manufactured and coated by HC Photonics. This crystal contains a single grating with a period of $8.61 \mu\text{m}$. Its faces are anti-reflection coated (reflection coefficient smaller than 0.5 %) for the pump, signal, idler wavelengths and are wedged by 1° to avoid étalon effects. It is designed to lead to quasi-phase matching conditions for a signal wavelength in the 776-796 nm range, depending on the temperature. The OPO cavity is a 1.095-m long ring cavity and consists in four mirrors. The two mirrors that sandwich the nonlinear crystal both have a 150 mm radius of curvature. The two other mirrors are planar. All mirrors are designed to exhibit a high reflectivity ($R \geq 99.9 \%$) between 776 nm and 796 nm and a transmission larger than 95 % at 532 nm and between 1605 nm and 1690 nm. This allows the OPO to be singly resonant, the resonant wave being the signal. The calculated waist of the signal beam at the middle of the PPSLT crystal is $43 \mu\text{m}$. The pump beam is focused by a 160 mm focal-length lens (L1) to a $35 \mu\text{m}$ radius waist inside the PPSLT crystal. Finally, to ensure stable single-frequency operation of the OPO, an uncoated YAG étalon is inserted in the second waist of the cavity. Different étalon thicknesses were tried, leading all to stable single-frequency operation of the OPO. In the following, the different results that are reproduced have been obtained either with a $150 \mu\text{m}$ thick or $250 \mu\text{m}$ thick étalon.

III. SRO PERFORMANCES

We first investigate the wavelength tuning characteristics of the OPO at a fixed pump power. For this measurement we use a spectrometer (AvaSpec 2048-2) to monitor the signal wavelength. The idler wavelength is then calculated based on energy conservation. The measured thermal tuning curves are reported in Fig. 2. One can see

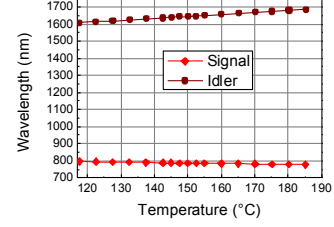


FIG. 2: Output signal and idler wavelengths versus PPSLT crystal temperature.

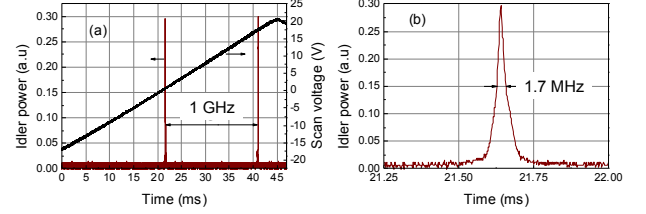


FIG. 3: (a) Observation of the idler spectrum using a scanning Fabry-Perot interferometer with a 1 GHz free spectral range. (b) Zoom on one of the peaks. The peak linewidth is limited by the Fabry-Perot finesse.

that the idler wavelength can be tuned from 1607.3 nm to 1686.09 nm (777.235 nm to 795.205 nm for the signal) when the PPSLT temperature is varied from 117.5°C to 185.2°C . The experimental slopes for the tunability of the OPO were estimated to be of $1.16 \text{ nm}/^\circ\text{C}$ for the idler and $-0.26 \text{ nm}/^\circ\text{C}$ for the signal, in reasonable agreement with the dispersion curves available in the literature [14].

In the following, we maintain the temperature of the PPSLT crystal at $T=152.5^\circ\text{C}$. This corresponds to a signal wavelength equal to 786 nm and an idler wavelength of 1646 nm. The OPO output beams are collimated with a 200 mm focal-length lens (L2). At this temperature, we check thanks to a 1 GHz free spectral range Fabry-Perot interferometer operating at the idler wavelength that the OPO stably oscillates on a single longitudinal mode. The corresponding signals can be seen in Fig. 3, with a $150 \mu\text{m}$ -thick étalon. One can clearly see in Fig. 3(a) that the OPO operates on a signal frequency. A zoom on one of the peaks shows that the peak full width at half maximum is equal to 1.74 MHz, which is actually limited by the finesse $F = 580$ of the Fabry-Perot.

We then measure the idler output power when the pump power is gradually decreased. Fig. 4 displays the obtained results. The plotted idler power corresponds to the one just at the output of mirror M2 of the OPO cavity. The pump power is measured just before the input concave mirror M1 of the cavity. We can see that a Watt level idler output power can be reached at 6.5 W pump power. At a pump power smaller than 4.5 W, the idler output power quickly drops. The OPO threshold is found to be equal to 2.5 W. This is comparable with the

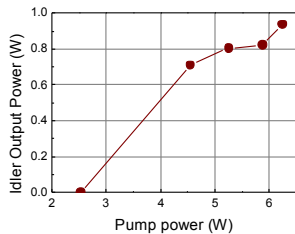


FIG. 4: Measured evolution of the idler output power versus pump power.

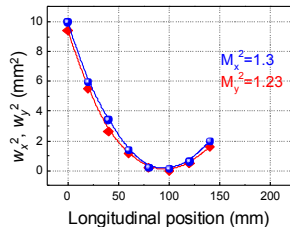


FIG. 5: Evolution of the square of the beam radius versus propagation distance in the two transverse dimensions x (resp. y) corresponds to the direction orthogonal to (resp. inside) the plane of the cavity. The full lines correspond to polynomial fits and the symbols to the experimental data.

threshold pump power we calculate using a simple truncated Gaussian beam model [15] with about 5 % round-trip losses for the signal. This threshold value could of course be decreased by decreasing the losses. For example, in the absence of intracavity étalon, we have checked that the threshold decreases below 1 W. However, since this would lead to lower conversion efficiencies at larger pump powers [16], we keep these losses in the following.

In order to check the spatial quality of the idler beam, we precisely measure its M^2 factor. To this aim, we measure the evolution of the beam radius when it is focused by a 150-mm focal length lens. Beam radii measurements are performed using the knife-edge method. From the experimental data we plot the square of the beam radius along the propagation axis and we perform a polynomial fit to recover the M^2 parameter in the two transverse directions, as shown in Fig. 5. As one can see, the idler beam is nearly diffraction limited. The slight discrepancy with respect to a perfect TEM_{00} mode is attributed to thermal effects in the PPSLT crystal.

IV. SPECTRAL PURITY, STABILITY, AND SERVO-LOCKING

Let us now focus on the noise properties of the OPO since this is a critical parameter in many quantum optics experiments. We focus on both the short-term spectral purity of the OPO (frequency noise, linewidth) and on its long term wavelength and power stability. In the fol-

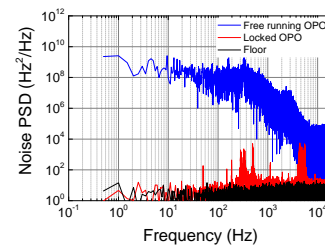


FIG. 6: Single-sided power spectral density of the frequency noise of the non resonant idler when the OPO is free running (blue) locked (red). The black spectrum is the measurement noise floor.

lowing, all experimental results were obtained at a pump power of approximately 5 W before L1 and a crystal temperature fixed at 152.5 ° C.

A. Spectral purity

We aim here at frequency locking the non-resonant idler of the OPO like in our previous work [11]. To this aim, we apply an error signal derived from the measured idler frequency noise to the OPO cavity length through a combination of a proportional-integral (PI) loop filter, a high-voltage amplifier and a piezoelectric transducer (Piezomechanik model PCh 150/5x5/2) carrying one of the cavity planar mirrors [11]. As sketched in Fig. 1, one part of the idler beam is sent to a medium finesse Fabry-Perot (FP) cavity (which acts as a frequency reference) after strongly attenuating its power with neutral density filters. A silicon plate is used to completely absorb the residual pump signal. The idler power incident on the FP cavity is equal to 500 μ W. The FP cavity is the same one as the one that was used to analyze the spectral purity of the OPO in Fig. 2 (1 GHz free spectral range and finesse $F = 580$ at the idler wavelength). We use this cavity to both measure the idler frequency noise and to stabilize it.

Preceding studies have shown that an OPO can be quite efficiently frequency stabilized by locking either on the side of the cavity transmission fringe [17] or on the top of the transmission fringe [18, 19]. The resulting frequency noise depends mainly on the reference cavity linewidth. Here, since the cavity linewidth (1.7 MHz) is not extraordinarily narrow, we just use the side-of-fringe locking technique, which does not require any Pound-Drever-Hall setup but only out-of-the shelf electronics. In free running mode, the OPO idler frequency is tuned to the side of the transmission peak of the cavity. The transmitted signal is recorded during 1 s using a deep memory oscilloscope. A fast Fourier transform algorithm is then used to compute the frequency noise spectrum of the non resonant idler, which is reproduced as the blue spectrum in Fig. 6. As expected, the spectrum of the idler frequency noise in the free running mode matches

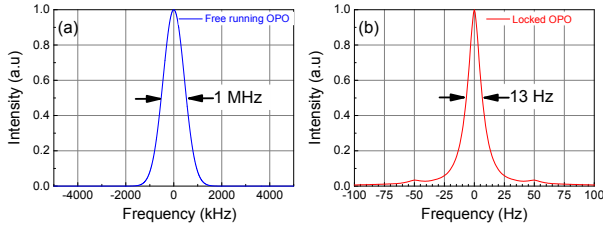


FIG. 7: Spectra of the non resonant idler field deduced from the frequency noise spectra of Fig. 6 in the (a) free running mode and (b) when it is locked.

quite well that of the pump frequency noise [17]. Moreover, since the bandwidth of the frequency noise is relatively low (about a few kHz), the use of a piezoelectric transducer carrying a cavity mirror to apply the correction signal should be fast enough. This is shown by the red spectrum in Fig. 6, which was obtained by recording the error signal during 2 seconds when the OPO is locked. This leads to a quasi white frequency noise in the considered frequency domain, with an average level of the order of a few Hz^2/Hz . The biggest noise peak is located at about 5 kHz frequency and reaches an amplitude equal to $10^3 \text{ Hz}^2/\text{Hz}$. It is due to a resonance of the piezoelectric actuator. The smaller peaks at lower frequencies (between 200 and 500 Hz) are reminiscent of the pump laser noise, not perfectly compensated by the servo-loop.

To calculate the root-mean-square (RMS) idler frequency noise relatively to the reference cavity, we integrate the noise power spectral density over the measurement bandwidth in both cases. In the free running regime, we obtain a RMS frequency noise of 445 kHz. When the OPO is locked with the PI corner frequency of the servo controller set at 3 kHz, the RMS frequency noise is equal to 570 Hz for an integration domain equal to [0.5 Hz, 15.5 kHz]. We have also calculated the idler spectrum by first computing the auto-correlation of the idler field $E(t)$ using the following expression [20, 21]:

$$R_E(\tau) \propto \exp \left[- \int_{-\infty}^{\infty} S_\nu(f) \frac{1 - \cos(2\pi f\tau)}{f^2} df \right], \quad (1)$$

where $S_\nu(f)$ is the power spectral density of the frequency noise. The spectrum of the OPO idler field can then be calculated by taking the Fourier transform of $R_E(\tau)$, as shown in Fig. 7. One can see that in free running regime, the OPO idler beam has a Gaussian lineshape with a linewidth of 1 MHz over 1 s. Such a spectrum is typical for a laser field affected by large frequency fluctuations at low Fourier frequencies. When the loop is closed, the frequency fluctuations of the OPO idler are strongly attenuated, leading to a more Lorentzian lineshape, which is consistent with the nearly white frequency noise spectrum in Fig. 6. The corresponding linewidth is then found to be equal to 13 Hz over 2 s. One

should not be surprised by the fact that the linewidth of the locked OPO is smaller than the RMS frequency noise value because the bandwidth considered here is about of 20 kHz, which is much larger than the RMS noise (570 Hz) [22, 23].

B. Influence of the intensity noise on the spectral purity

It is well known that a serious drawback of the side-of-fringe locking technique with respect to the Pound-Drever-Hall locking technique is that the former one is not immune to intensity fluctuations: any intensity fluctuation could be wrongly attributed to frequency fluctuations and lead the servo-lock to introduce extra frequency noise [18]. It is thus of paramount importance to measure the intensity fluctuations and to quantify their influence on the frequency fluctuations of the locked OPO. To this aim, we recorded the idler intensity noise of the free running OPO. We recorded this intensity noise with the same detector as the one used after the reference Fabry-Perot cavity, and we attenuated the detected intensity in such a way that it is equal to the average intensity detected after the reference cavity when the OPO is locked. Figure 8 compares the spectrum of this intensity noise with the error signal noise when the OPO is locked. We can see that the intensity noise of the free running OPO is slightly larger than the error signal noise when the OPO is locked. This means that the servo loop converts a small fraction of the OPO intensity noise into unwanted frequency fluctuations. In order to investigate the order of magnitude of this conversion, we write the photocurrent noise $\delta i(t)$ as the sum of two terms:

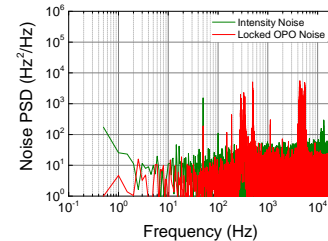


FIG. 8: Single-sided power spectral density of the intensity noise of the non resonant idler when the OPO is free running (green) and of the detected error signal when the OPO is locked (red).

$$\delta i(t) = \eta [\delta P(t) + P_0 K \delta \nu(t)], \quad (2)$$

where η is the response of the detector, P_0 is the average detected power, $\delta P(t)$ holds for the power fluctuations, K is the frequency to power conversion factor of the reference cavity, and $\delta \nu(t)$ represents the frequency noise of the OPO. In eq. (2), the first term comes from power

fluctuations and the second one from frequency fluctuations. We have also supposed in this equation that the fluctuations are small enough to allow us to keep only linear terms. In free-running mode, i. e. when the OPO frequency is not locked, comparison of the blue spectrum of Fig. 6 with the green spectrum of Fig. 8 shows that the frequency fluctuations dominate over the intensity fluctuations: the first term of eq. (2) can be neglected. However, comparison of the two spectra of Fig. 8 shows that this is no longer the case when the OPO is locked. If we suppose that the servo-lock is perfect and that the total photocurrent noise in eq. (2) is zero at the considered frequencies, eq. (2) gives a majorant to the frequency noise created at a given frequency f by transfer from the intensity noise:

$$S_{\delta\nu}(f) = \frac{1}{K^2 P_0^2} S_{\delta P}(f), \quad (3)$$

where $S_{\delta P}(f)$ and $S_{\delta\nu}(f)$ are the power spectral densities of the power and frequency fluctuations at frequency f , respectively. From Fig. 8, we can see that the intensity noise is approximately 3 dB above the frequency noise. This means that the linewidth of Fig. 6(b) is underestimated by a factor of approximately two. We can thus conclude that the linewidth of the locked OPO, with respect to the reference cavity, is of the order of 30 Hz over 2 s. This means that, even taking the detrimental effect of intensity noise into account, we have been able to decrease the linewidth of the non resonant idler by more than four orders of magnitude, well below the sub-kHz level.

To the best of our knowledge, this is the smallest linewidth ever achieved using an OPO without implementing a Pound-Drever-Hall stabilization scheme with a higher finesse cavity [24]. Of course, this linewidth is the relative linewidth with respect to the reference cavity, and any long term drift of the cavity will be transferred to the OPO idler, as we are going to investigate now.

C. Long term stability

The idler frequency long term stability is analyzed by using a 0.01 pm resolution wavelength meter (Angstrom WS7 from HighFinesse GmbH, see Fig. 1). A typical result obtained when the OPO is free running (servo-locking OFF) is reproduced in Fig. 9, for a 250- μ m-thick étalon. This result shows that the free-running OPO typically experiences one mode-hop per hour. In the case reproduced in Fig. 9, this mode hop corresponds to a few longitudinal modes.

Once locked to the cavity, the idler frequency should become much more stable. This is what is observed in Fig. 10. The OPO remains locked for 45 min, without any mode hop. During this time, the idler frequency drifts by 500 MHz. This is due to the fact that the FP reference cavity, which is not thermally stabilized, is of course not an absolute frequency reference. This 500 MHz frequency

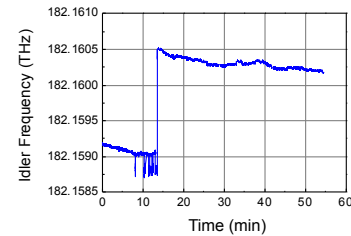


FIG. 9: Long-term evolution of the non resonant idler frequency versus time in the free running mode.

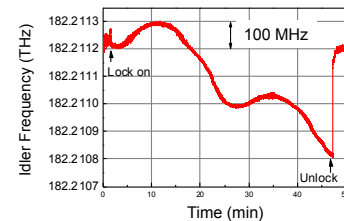


FIG. 10: Evolution of the non resonant idler frequency versus time in the locked mode.

excursion corresponds to a temperature variation of a fraction of a degree, which is perfectly plausible in our lab environment.

We also checked the power stability of the emitted idler, both on free running and frequency locked conditions (see Fig. 11). The relative RMS power fluctuations are equal to 0.8 % in both the free running and locked modes. The frequency stabilization does not alter power stability, as expected.

V. CONCLUSION

In conclusion, we have demonstrated a cw SRO with output power of the order of 1 Watt in the 1600–1700 nm wavelength domain and with a linewidth narrowed down to the sub-kHz level by external locking to the side of the transmission peak of a Fabry-Perot reference cavity. With its ultra narrow linewidth (about 30 Hz over 2 s)

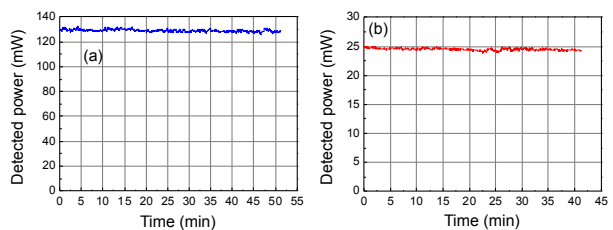


FIG. 11: Time evolution of the non resonant idler power in (a) free running mode and (b) frequency locked regime.

combined to its good long term stability (frequency and power), this laser source could be a good candidate to pump quantum interfaces necessary for quantum communication applications. Future development will include the thermal stabilization of the overall setup, and in particular the reference Fabry-Perot cavity. Better long term frequency stabilization can also be expected thanks to the use of a volume Bragg grating to replace one cavity mirror [26]. Finally, short term frequency fluctuations could also be reduced, together with immunity to intensity noises, by implementing a Pound-Drever-Hall lock-

ing scheme [24] with a higher finesse cavity [18], although this is probably not necessary for our quantum interface application.

Acknowledgment

The authors are happy to thank S. Tanzilli and F. Kaiser for helpful discussions, and L. Morvan for technical assistance.

-
- [1] F. Bussi eres, N. Sangouard, M. Afzelius, H. de Riedmatten, C. Simon, and W. Tittel, "Prospective applications of optical quantum memories," *J. Mod. Opt.* **60**, 1519-1537 (2013).
 - [2] P. Kumar, "Quantum frequency conversion," *Opt. Lett.* **15**, 1476-1478 (1990).
 - [3] S. Tanzilli, W. Tittel, M. Halder, O. Alibart, P. Baldi, N. Gisin, and H. Zbinden, "A photonic quantum information interface," *Nature* **437**, 116-120 (2005).
 - [4] N. Maring, K. Kutluer, J. Cohen, M. Cristiani, M. Mazzer, P. M. Ledingham, and H. de Riedmatten, "Storage of up-converted telecom photons in a doped crystal," *New Journal of Physics* **16**, 113021-113037 (2014).
 - [5] Y. -H. Cheng, T. Thomay, G. S. Solomon, A. L. Migdall, and S. V. Polyakov, "Statistically background-free, phase-preserving parametric up-conversion with faint light," *Opt. Express* **14**, 18671-18678 (2015).
 - [6] C. E. Vollmer, C. Baune, A. Samblowski, T. Eberle, V. H andchen, J. Fiur asek, and R. Schnabel, "Quantum up-conversion of squeezed vacuum states from 1550 to 532 nm," *Phys. Rev. Lett.* **112**, 073602-073607 (2014).
 - [7] J.S. Pelc, L. Ma, C.R. Phillips, Q. Zhang, C. Langrock, O. Slattery, X. Tang, and M. M. Fejer, "Long-wavelength-pumped upconversion single-photon detector at 1550 nm: performance and noise analysis," *Opt. Express* **19**, 21445-21456 (2011).
 - [8] P. S. Kuo, J. S. Pelc, O. Slattery, Y.-S. Kim, M. M. Fejer, and X. Tang, "Reducing noise in single-photon-level frequency conversion," *Opt. Lett.* **38**, 1310 (2013).
 - [9] J. S. Pelc, Q. Zhang, C. R. Phillips, L. Yu, Y. Yamamoto, and M. M. Fejer, "Cascaded frequency upconversion for high-speed single-photon detection at 1550 nm," *Opt. Lett.* **37**, 476-478 (2012).
 - [10] G.-L. Shentu, J. S. Pelc, X.-D. Wang, Q.-C. Sun, M.-Y. Zheng, M. M. Fejer, Q. Zhang, and J.-W. Pan, "217 km long distance photon-counting optical time-domain reflectometry based on ultra-low noise up-conversion single photon detector," *Opt. Express* **21**, 13986-13991 (2013).
 - [11] A. Ly, B. Szymanski, and F. Bretenaker, "Frequency stabilization of the non-resonant wave of a continuous-wave singly resonant optical parametric oscillator," *Appl. Phys. B* **120**, 201-205 (2015).
 - [12] I. Ricciardi, S. Mosca, M. Parisi, P. Maddaloni, L. Santamaria, P. De Natale, and M. De Rosa, "Sub-kilohertz linewidth narrowing of a mid-infrared optical parametric oscillator idler frequency by direct cavity stabilization," *Opt. Lett.* **40**, 4743-4746 (2015).
 - [13] I. Silander, T. Hausmaninger, W. Ma, F. J. M. Harren, and O. Axner, "Narrowing of the linewidth of an optical parametric oscillator by an acousto-optic modulator for the realization of mid-IR noise-immune cavity-enhanced optical heterodyne molecular spectrometry down to $10^{-10} \text{ cm}^{-1} \text{ Hz}^{-1/2}$," *Opt. Lett.* **40**, 439-442 (2015).
 - [14] A. Bruner, D. Eger, M. B. Oron, P. Blau, M. Katz, and S. Ruschin, "Temperature-dependent Sellmeier equation for the refractive index of stoichiometric lithium tantalate," *Opt. Lett.* **28**, 194-197 (2003).
 - [15] R. L. Sutherland, *Handbook of nonlinear optics, 2nd edition* (Marcel Dekker, New York, 2003).
 - [16] I. Breuning, D. Haertle, and K. Buse, *Appl. Phys. B: "Continuous-wave optical parametric oscillators: recent developments and prospects," Lasers Opt.* **105**, 99-112 (2011).
 - [17] O. Mhibik, T.-H. My, D. Pab euf, F. Bretenaker, and C. Drag, "Frequency stabilization at the kilohertz level of a continuous intracavity frequency- doubled singly resonant optical parametric oscillator," *Opt. Lett.* **35**, 2364-2366 (2010).
 - [18] O. Mhibik, D. Pab euf, C. Drag, and F. Bretenaker, "Sub-kHz-level relative stabilization of an intracavity doubled continuous wave optical parametric oscillator using Pound-Drever-Hall scheme," *Opt. Express* **19**, 18047-18057 (2011).
 - [19] E. Andrieux, T. Zanon, M. Cadoret, A. Rihan, and J.-J. Zondy, "500 GHz mode-hop-free idler tuning range with a frequency-stabilized singly resonant optical parametric oscillator," *Opt. Lett.* **36**, 1212-1214 (2011).
 - [20] D. Middleton, *An introduction to statistical communication theory* (McGraw-Hill, New York, 1960).
 - [21] D. S. Elliott, R. Roy, and S. J. Smith, "Extracavity laser band-shape and bandwidth modification," *Phys. Rev. A* **26**, 12-18 (1982).
 - [22] O. Svelto et al., in *Springer handbook of lasers and optics*, F. Tr ager, ed., ch. 11 (Springer, New York, 2007).
 - [23] G. Di Domenico, S. Schilt, and P. Thomann, "Simple approach to the relation between laser frequency noise and laser line shape," *Appl. Opt.* **49**, 4801-4807 (2010).
 - [24] R. W. P. Drever, J. L. Hall, F. V. Kowalski, J. Hough, G. M. Ford, A. J. Munley, and H. Ward, "Laser phase and frequency stabilization using an optical resonator," *Appl. Phys. B* **31**, 97-105 (1983).
 - [25] Ch. Salomon, D. Hils, and J. L. Hall, "Laser stabilization

- at the millihertz level,” J. Opt. Soc. Am. B **5**, 1576-1587 (1988).
- [26] P. Zeil, N. Thilmann, V. Pasiskevicius, F. Laurell, Opt. Express **22**, 29907-29913 (2014).